

Proceedings of the ASME 2018
Conference on Smart Materials, Adaptive Structures and Intelligent Systems
SMASIS2018
September 10-12, 2018, San Antonio, TX, USA

SMASIS2018-8170

A LEADING-EDGE ALULA-INSPIRED DEVICE (LEAD) FOR STALL MITIGATION AND LIFT ENHANCEMENT FOR LOW REYNOLDS NUMBER FINITE WINGS

Mihary R. Ito

Department of Mechanical Science and Engineering Bio-Inspired Adaptive Morphology Lab University of Illinois Urbana-Champaign Urbana, Illinois 61801 Email: mri2@illinois.edu

Leonardo P. Chamorro

Department of Mechanical Science and Engineering Renewable Energy & Turbulent Environment Group University of Illinois Urbana-Champaign Urbana, Illinois 61801 Email: lpchamo@illinois.edu

Chengfang Duan

Department of Mechanical Science and Engineering Bio-Inspired Adaptive Morphology Lab University of Illinois Urbana-Champaign Urbana, Illinois 61801 Email: cduan3@illinois.edu

Aimy A. Wissa *

Department of Mechanical Science and Engineering Bio-Inspired Adaptive Morphology Lab University of Illinois Urbana-Champaign Urbana, Illinois 61801 Email: awissa@illinois.edu

ABSTRACT

Even though Unmanned Aerial Vehicles (UAVs) operating at low Reynolds numbers are becoming common, their performance and maneuverability are still greatly limited due to aerodynamic phenomena such as stall and flow separation. Birds mitigate these limitations by adapting their wings and feather shapes during flight. Equipped with a set of small feathers, known as the alula, located near the leading edge and covering 5% to 20% of the span, bird wings can sustain the lift necessary to fly at low velocities and high angles of attack. This paper presents the effect on lift generation of different placements of a Leading-Edge Alula-inpsired Device (LEAD) along the span of a moderate aspect-ratio wing. The device is modeled after the alula on a bird, and it increases the capability of a wing to maintain higher pressure gradients by modifying the near-wall flow close to the leading-edge. It also generates tip vortices that

modify the turbulence on the upper-surface of the wing, delaying flow separation. The effect of the LEAD can be compared to traditional slats or vortex generators on two-dimensional wings. For finite wings, on the other hand, the effect depends on the interaction between the LEADs tip vortices and those from the main structure. Wind tunnel experiments were conducted on a cambered wing at post-stall and deep-stall angles of attack at low Reynolds numbers of 100,000 and 135,000. To quantify the aerodynamic effect of the device, the lift generated by the wing with and without the LEAD were measured using a 6-axis force and torque transducer, and the resulting lift coefficients were compared. Results show that the location of the LEAD yielding the highest lift enhancement was 50% semi-span away from the wing root. Lift improvements of up to 32% for post stall and 37% for deep stall were obtained at this location, demonstrating that the three-dimensional effects of the LEAD are important. The lift enhancement was also more prominent

^{*}Address all correspondence to this author.

on a finite moderate aspect-ratio wing (3D) than on an airfoil (2D), confirming that the LEAD is a three-dimensional device. Identifying the configurations and deployment parameters that improve lift generation the most is needed to design an adaptive LEAD that can be implemented on a UAV wing for increased mission-adaptability.

Nomenclature

α	Wing An	gle of Attac	ck (AOA)
----------	---------	--------------	----------

 α_{STALL} Wing Stall AOA α_{ZL} Zero-Lift AOA R Wing Aspect Ratio

β LEAD AOA Relative to Wing Chord Line

γ LEAD Tip Deflection Angle

Wing Span b LEAD Span b_A Wing Chord cLEAD Chord c_A 3D Lift Coefficient C_L C_l 2D Lift Coefficient Alula Length L_A Bird Span L_b

 L_c Alula Root to Wingtip Distance

 L_w Extended Wing Length Re Reynolds number

 y_A LEAD Root to Wing Root Distance (%)

 C_{L0} 3D Baseline Lift Coefficient C_{l0} 2D Baseline Lift Coefficient

 $C_{L\alpha}$ 3D Lift-Curve Slope $C_{l\alpha}$ 2D Lift-Curve Slope

1 INTRODUCTION

Over the past decade, the use of Unmanned Aerial Vehicles (UAVs) has expanded beyond military applications. In fact, UAVs can now be encountered in countless commercial and research applications. In these areas, the vehicles have small characteristic lengths, operate in confined spaces as well as close to humans, and are assigned various tasks that demand high maneuverability. Therefore, safety and mission adaptability, defined as the ability to successfully complete multiple tasks (simple or complex) using the same vehicle, are important design factors. In nature, mission adaptability is encountered in avian flight as birds engage in complex maneuvers such as take-off, landing, diving, gliding, perching, and hovering using the same flight apparatus. Both bird wings and UAV wings with conventional airfoils operate at low Reynolds numbers, which is characterized by low speeds and small flight surfaces [1]. However, the flight envelope of UAVs at low Reynolds numbers is currently not as large as it is for birds due to aerodynamic limitations, which greatly contributes to mission adaptability. According to aerodynamic principles, the best method to produce high lift at low speeds is to increase the lifting surface's angle of attack. However, this angle can only be increased up to the stall angle of attack, α_{STALL} , beyond which lift generation is limited by flow separation [2] [3]. Therefore, alternative methods to generate high lift at low Reynolds numbers are necessary to achieve mission-adaptability.

This paper proposes a Leading-Edge Alula-inpsired Device (LEAD) as a lift-enhancement and stall-mitigation device for finite wings with low to moderate aspect ratios operating at low Reynolds numbers. In this paper, the authors seek to understand the effect of varying the LEAD root location along the wing span on lift generation. It also addresses how well the device performs on a moderate aspect ratio wing (3D) compared to an airfoil (2D). Understanding the LEAD configurations that enhance lift and mitigate stall the most is crucial to develop an adaptive design for the device.

2 BACKGROUND AND PREVIOUS WORK

2.1 High-lift Aerodynamics, Leading Edge Devices

Currently, high-lift devices, such as flaps, slats, and vortex generators, are used to enhance lift and to delay separation on lifting surfaces operating at both low and high Reynolds numbers [4]. A lifting surface equipped with these devices generates sufficient lift to stay airborne at low velocities and high angles of attack. This is typically achieved by modifying the chord and the camber of the airfoil of the lilting surface or by modifying the boundary layer surrounding it [5]. Devices currently in use on aircrafts include trailing edge flaps, which are used to modify a wing's chord and camber to delay stall [6]. Devices that modify the boundary layer surrounding the wing include vortex generators, which create vortices that energize the boundary layer over the upper surface of a wing [7]. Aircrafts also use leading-edge slats, which modify the adverse pressure gradient on the wing's airfoil such that they are less prone to stall [8]. Currently, these devices are well-suited for large aircrafts; hence, they are large, heavy, and actuated by complex mechanisms. Therefore, further investigation is necessary to design adequate high lift devices for small-scale UAVs.

2.2 Alula in Avian Flight

Birds have a high-lift device located near the wing leadingedge called the alula feather structure. The alula, also known as 'bastard wing', is comprised of 2 to 6 feathers and allows the bird to fly at low speeds and high angles of attack. In cruising conditions, it remains stowed along the upper surface of the wing near the leading-edge. During high angle of attack maneuvers, such as take-off, landing, and perching, the alula has been observed to deploy away from the wing upper surface. Previous studies by biologists on the role of the alula in bird flight concluded that the feather structure delays flow reversal on the surface of a wing flying at high angles of attack [9], [10], [11], [12].

Bird wings have been classified into four types (A, B, C, and D) by Saville et al. [13]:

- 1. Type A, elliptical wings, are most common in birds that fly in confined environments, such as forests.
- 2. Type B, high-speed wings, are encountered in migratory birds that fly at higher speeds and open spaces.
- 3. Type C, high aspect-ratio wings, are typical in birds that fly over water and long-distances without needs to frequently take-off and land.
- 4. Type D, high-lift wings, and best-suited for birds of prey which fly at low speeds and frequently take-off, land, and perch. The airfoils of these wings are highly cambered [14], and their alulae are larger than those on other wing types.

Alvarez et al. [15] investigated the characteristics of alulae on various bird species equipped with these four types of wings and compiled their results in a detailed database. The results of this study confirmed that birds equipped with type D wings exhibit the most pronounced alulae. Table 1 shows a summary of the type D wings and alulae dimensions of the species evaluated. As recorded in table 1, the length, or span, of the alula for high lift wings ranges from 14.4% to 19.4% of the full bird span. With respect to the wing root, the alula root for a high lift wing is located between 28.6% and 41.4% semi-span away.

Morphologically, the alula is located at the joint between the hand-wing and the arm-wing of birds as shown in figure 1 [16]. The arm wing is located inboard of the alula and is comprised of large bones and muscles, providing mechanical support to the wing. Due to its structure, the cross-sections in this portion of the wing consist of thicker airfoils. Smoother adverse pressure gradients form around this region, making it suitable for low speed flight. The hand wing is located outboard of the alula and mostly consists of feathers, structures that are thinner and more flexible that bones. This portion of the wing is comprised of thinner airfoils that are well-suited for high speeds [10]. Since a type D wing is well-adapted to low speed flight, its arm wing is large, and the alula is located further outboard than on wings of other types [15]. Due to these factors, birds equipped with Type D wings depend on the effects of their pronounced alulae to achieve mission adaptability.

2.3 Alula in Engineering (2D)

While the role of the alula in avian flight has been investigated by many researchers, the first implementation of an engineered alula device (LEAD) for lift enhancement and stall mitigation can only be found in an experimental study conducted by the authors on a cambered airfoil equipped with the LEAD

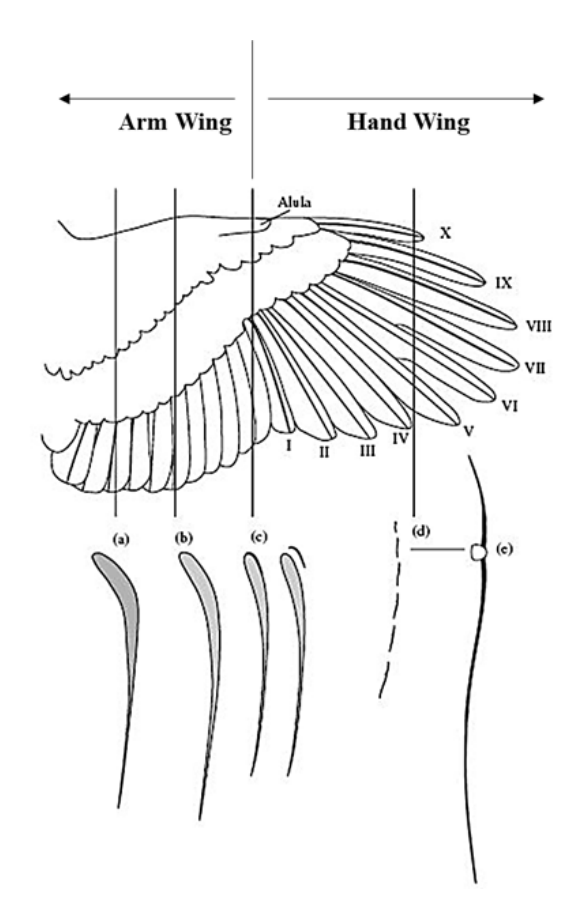


FIGURE 1. Schematic of a goshawk wing with cross-sections at various spanwise positions. The thickest airfoil-like sections are located at the wing root and become thinner toward the tip. Adapted from Videler [16].

at low Reynolds numbers [17] [18]. The results of this study have shown that the LEAD affects the airflow in two main ways. First, it modifies the boundary layer near the wing leading-edge to increase the capacity of the airfoil to sustain higher pressure gradients. This effect is also known as the slat effect. Second, the alula generates a tip-vortex that produces a streamwise flow on the upper surface of the wing. This tip-vortex effect adds momentum to the flow and delays flow separation at steep angles of attack. An airfoil equipped with the LEAD as presented by Mandadzhiev et al. [18] produces more lift and delays flow separation.

Since the alula is typically found on birds with low and moderate aspect-ratios, a 2D experiment gives an insightful but incomplete picture on the implementation of the LEAD on a lifting surface. Therefore, an experiment on a finite wing is necessary to further understand the aerodynamic effects of the device.

Bird Species	Alula Length	Wing Aspect Ratio	Alula Root to Wing Tip	Alula Length to Bird Span
	L_a [m]	AR	Distance L_C/L_W	Ratio $2L_a/L_b$
Bubulcus ibis	0.07	7.239	0.600	0.169
Ciconia ciconia	0.14	8.402	0.586	0.146
Milvus migrans	0.11	7.465	0.678	0.158
Gyps fulvus	0.16	6.345	0.653	0.144
Hieraaetus pennatus	0.11	7.403	0.669	0.182
Falco naumanni	0.05	8.03	0.714	0.152
Tyto alba	0.07	7.689	0.654	0.156
Otus scops	0.04	5.886	0.633	0.194
Athene noctua	0.04	5.784	0.665	0.188
Strix aluco	0.07	6.198	0.645	0.175
Average	0.09	7 004	0.649	0.166

TABLE 1. Database of Type D (High-Lift) Wings as Recorded by Alvarez et al. [15]

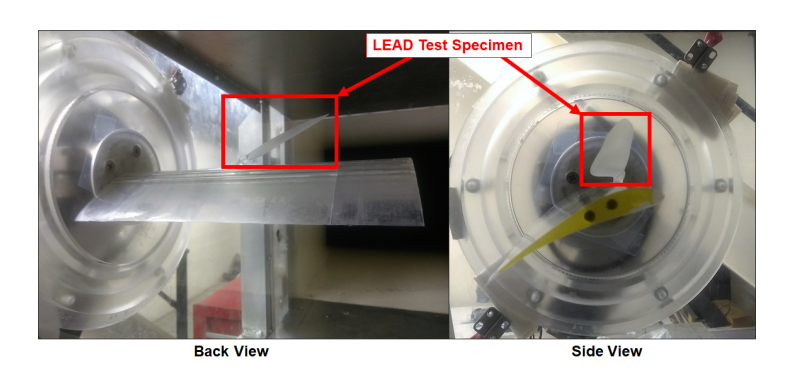


FIGURE 2. Wind Tunnel Experiment Setup of Rectangular Wing with s1223 Airfoil Cross-Section Equipped with LEAD Specimen.

3 EXPERIMENTAL SETUP

Wind-tunnel experiments were performed to measure the lift generated by a moderate aspect ratio wing. Measurements at low Reynolds numbers were taken for a baseline configuration and for wing equipped with a LEAD. The tests were conducted in an open-loop wind tunnel at University of Illinois Urbana-Champaign. The wind tunnel has four test sections of expanding areas to minimize streamwise pressure gradients. The first section, which is closest to the wind tunnel inlet, was chosen for the experiment due to the low boundary layer thickness and turbulence levels. The cross-section is rectangular with a height of 0.45m and a width of 0.9m. To measure the lift generated, the wing-LEAD assembly was firmly mounted to an ATI Gamma 6-axis force transducer. The test apparatus was then mounted to the side wall of the wind tunnel as shown as figure 2.

3.1 Wing and LEAD Test Specimens

To achieve similar aerodynamic effects as the wing shapes and alula morphological parameters observed in the bird species discussed previously (table 1), the semi-span (distance from wing root to tip, b/2) for the test specimen was set to 220mm,

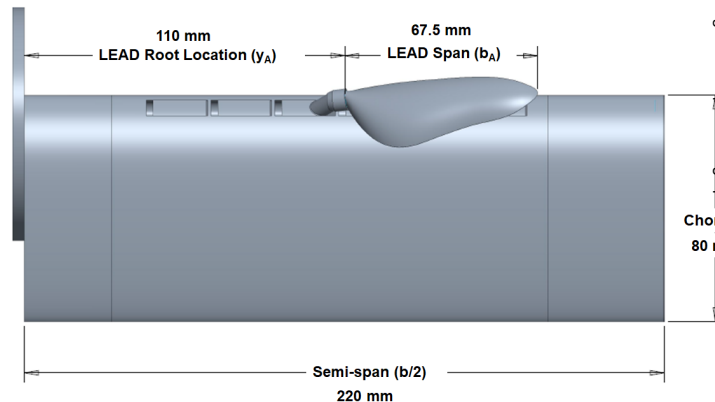
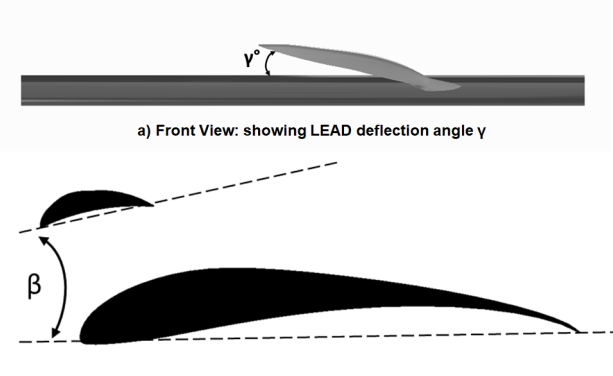


FIGURE 3. Model of rectangular test wing equipped with LEAD specimen showing the LEAD root at the $y_A = 50\%$ location.

the chord (c) to 80mm, and the wing aspect ratio (AR) was 5.5. The selected airfoil for this wing was the S1223, which has a maximum thickness of 12.1% at 19.8% of the chord and a maximum camber of 8.1% at 49% of the chord. This high-lift and highly cambered airfoil is similar to typical type D wing profiles [14] [19].

The LEAD test specimen covered 15% of the wing span, with a mean chord (c_a) of 18.7mm and a span (b_A) of 67.5mm. The wing was designed with slots in which the LEAD specimen can be secured at different locations (y_A) along the span. A model of the rectangular wing equipped with the LEAD are shown in figure 3. Additionally, the tip of the LEAD specimen was deflected at an angle γ with respect to the wing upper surface and the LEAD chord was set to an angle of attack β relative to the main wing's chord for all measurements conducted. The airfoil profiles, the LEAD relative angle of attack (β) , and the tip deflection angle (γ) are defined in figure 4 and their values were varied as summarized in 3.2.





b) Side View: showing wing cross-section and LEAD angle of attack β

FIGURE 4. Illustration of the wing-LEAD assembly showing the tested geometric parameters β and γ . Adapted from Mandadzhiev et al. [18].

3.2 **Experiment Matrix**

The wind speed in the wind tunnel was varied to produce low Reynolds numbers of 100,000 and 135,000. The wing angle of attack (α) was varied from -10° to 40° in increments of 1° to obtain the baseline lift coefficients. Since the LEAD is a poststall device [17], the LEAD and wing assembly was evaluated only at high angles of attack (α) of 18°, 26°, and 34°.

The following LEAD geometric parameters were tested:

- LEAD AOA relative to wing chord: $\beta = -18^{\circ}$, -13° , -10° ,
- LEAD tip deflection angle: $\gamma = 4^{\circ}$, 13° , 22° ,
- Distance from wing root to LEAD root, as a percentage of the semi-span (b/2): $y_A = 30\%$, 40%, 50%, 60%, 70%.

4 **RESULTS**

Since the wing evaluated in this experiment is finite with a moderate aspect ratio, three-dimensional corrections were applied to the linear region of the two-dimensional C_l vs. α curves to validate finite wing lift curve slope. The change in lift-curve slope is based on the wing aspect ratio and is given by equation 1 [1]. The baseline lift coefficient obtained at each angle of attack as shown in figure 5, validating the experimental data against published C_l vs. α curves for the s1223 airfoil [20].

$$C_{L\alpha} = C_{l\alpha} \frac{AR}{(AR+2)} \tag{1}$$

The baseline lift coefficients used to compute the lift improvements due to the LEAD are marked at each angle of attack of interest as shown in figure 6.

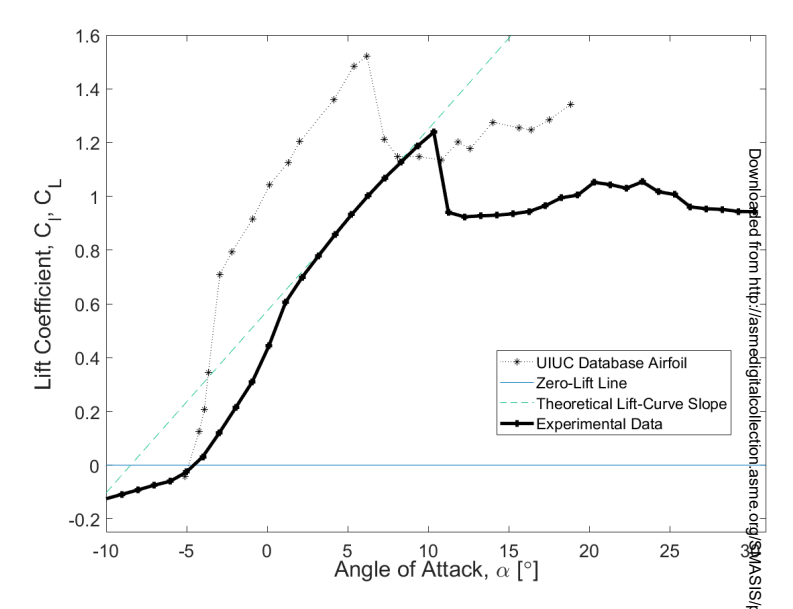


FIGURE 5. Validation of 3D experimental results at Re = 100,000 against the s1223 airfoil data published by Selig et al. in [20].

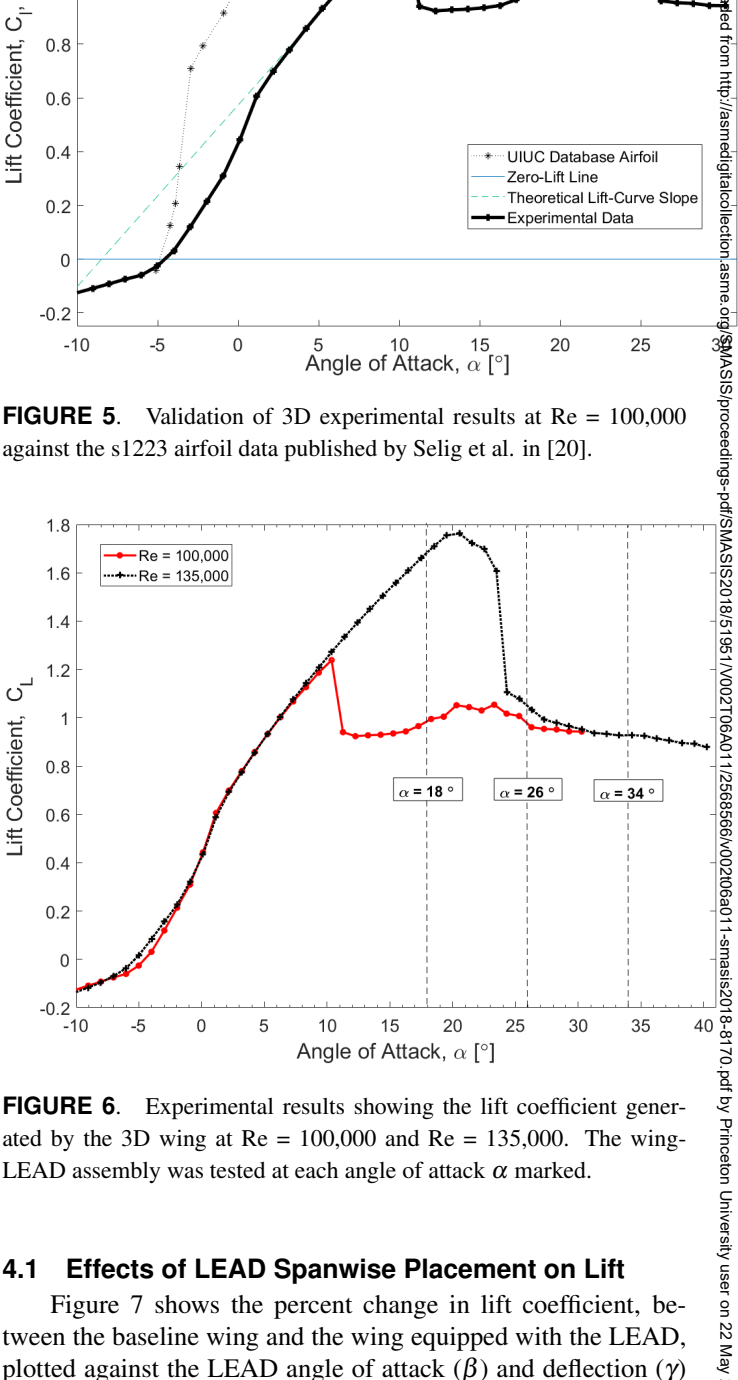


FIGURE 6. Experimental results showing the lift coefficient generated by the 3D wing at Re = 100,000 and Re = 135,000. The wing-LEAD assembly was tested at each angle of attack α marked.

4.1 Effects of LEAD Spanwise Placement on Lift

Figure 7 shows the percent change in lift coefficient, between the baseline wing and the wing equipped with the LEAD, plotted against the LEAD angle of attack (β) and deflection (γ) at Re = 100,000. The plots shown are main effect plots; thus, the contribution of only one geometric parameter is presented while the second parameter is averaged (e.g. the top plots show

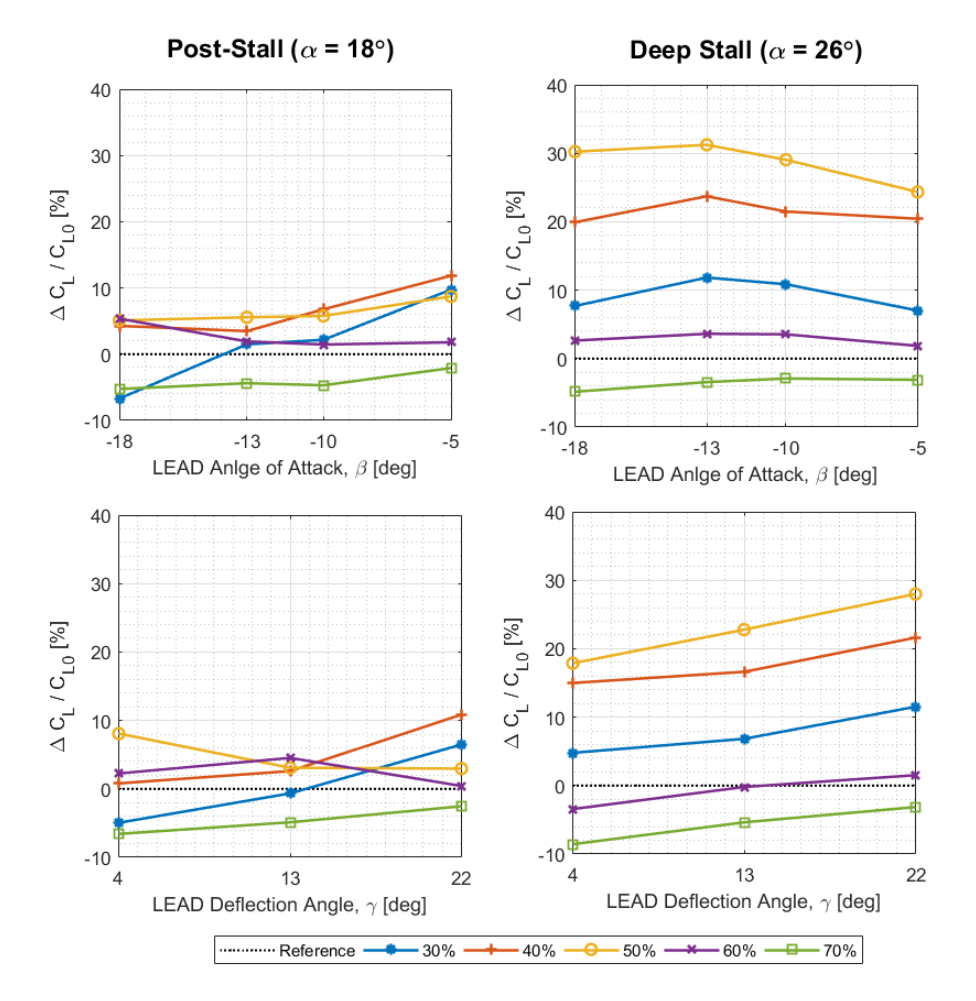


FIGURE 7. Percent difference in lift coefficients generated by the baseline wing and the wing-LEAD assembly (Main Effects) at Re = 100,000.

 $%C_L$ vs. β with averaged γ values at different locations y_a). The results indicate that the LEAD increased the lift generated by the wing at post-stall ($\alpha = 18^{\circ}$) and deep stall ($\alpha = 26^{\circ}$) angles of attack. The greatest increase in lift due to the LEAD was to 32% and occurred when the wing is in deep stall. This highest increased was obtained when the LEAD was placed 50% semispan away from the wing root. Once the device was moved further outboard of this location, however, the lift enhancement declined but still remained favorable. Once the LEAD has reached the most outboard location (70% semi-span away from the wing root), the LEAD tip protruded outboard of the wing tip, and all configurations generated lift coefficients lower than the baseline. For all locations, a LEAD relative angle of attack of $\beta = -5^{\circ}$ resulted in the greatest lift enhancement at post-stall, whereas β = -13° performed best in deep stall. Furthermore, under all stall conditions and at all locations, a tip deflection of $\gamma = 22^{\circ}$ consistently yielded the highest increase in lift coefficient at most angles of attack.

The performance for the same geometric parameters at Re=135,000 is shown in figure 8. In this case, the wing stall angle α_{STALL} increased from 10° to 20° . As a result, $\alpha=18^{\circ}$ became a pre-stall angle of attack, so $\alpha=26^{\circ}$ was labeled post-stall and $\alpha=34^{\circ}$ deep-stall. The results obtained were similar to Re=100,000, except the location yielding the best performance was $y_A=60\%$ in the post-stall condition. Additionally, the greatest increase in lift, up to 37%, produced by the LEAD occurs when the wing is in post-stall. Similarly to Re=100,000 results, lift enhancements declined as the LEAD was moved outboard of the location of highest improvement. Furthermore, a tip deflection of $\gamma=22^{\circ}$ and relative angle of attack of $\beta=-13^{\circ}$ consistently increased the lift coefficient the most at all locations and angles of attack.

4.2 LEAD as a Three-Dimensional Device

To evaluate the LEAD as a three-dimensional device, the improvements in lift coefficient obtained at the location (y_A) yield-

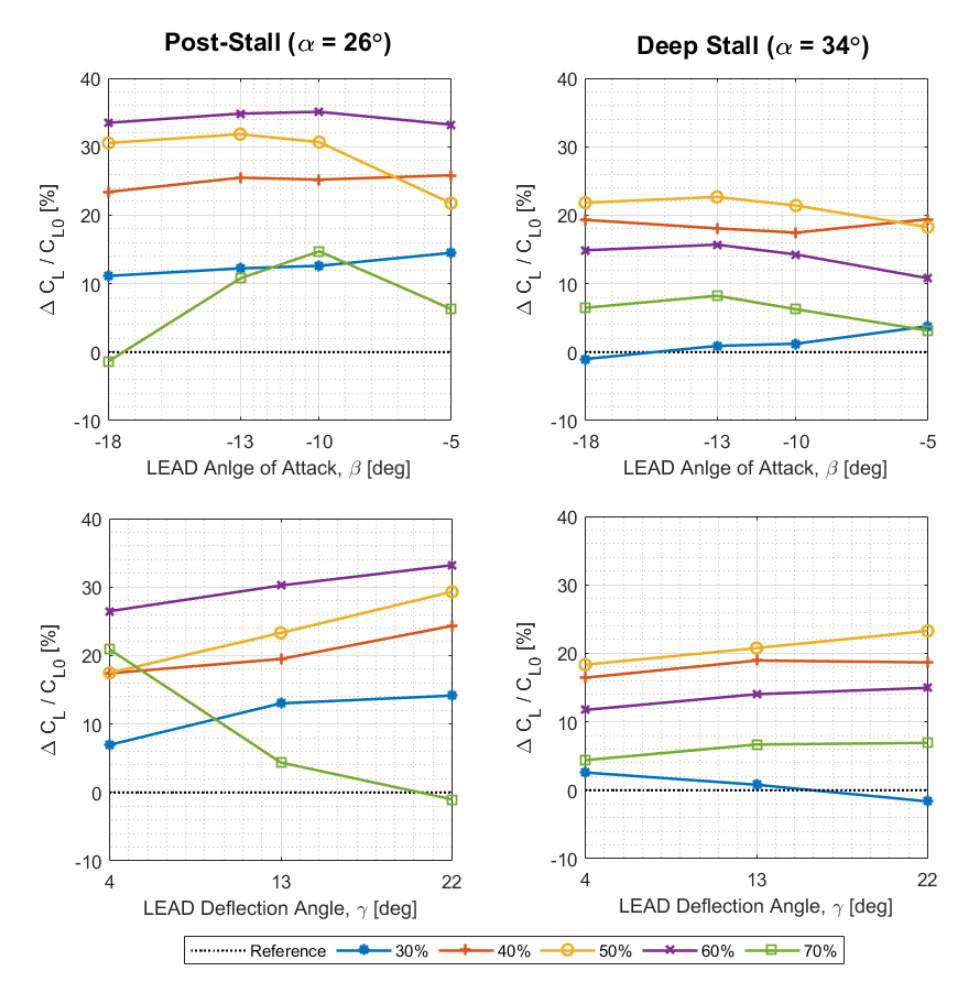


FIGURE 8. Percent difference in lift coefficients generated by the baseline wing and the wing-LEAD assembly (Main Effects) at Re = 135,000.

ing the highest increased were compared to the results obtained in the airfoil configuration as tested by the authors in [17] for a given Reynolds number and stall conditions. The results shown in figure 9 indicate that the device enhanced the lift coefficient generated by the wing for both cases. However, the finite wing with a LEAD generated a higher percent lift difference compared to its airfoil counterpart. At Re = 100,000, the LEAD on an airfoil yielded C_L improvements ranging from 1% to 5% in both post-stall and deep stall conditions. While the LEAD on a finite wing improved the lift coefficient within ranges similar to the airfoil configuration at post-stall, the results show that it enhanced C_L significantly more with a range of 9% to 32% in deep stall. At Re = 135,000, the airfoil configuration yielded a higher increase in lift, ranging from 11% to 22% in post-stall compared to Re =100,000. The finite wing configuration, on the other hand, generated an increase of 11% to 29%. Overall, the results show higher lift enhancement when the LEAD is placed on a finite wing as opposed to an airfoil.

5 DISCUSSION

Based on the results obtained, the LEAD is a post-stall liftenhancing device when placed on the leading edge of a finite wing of moderate aspect-ratio. In fact, for most configurations tested, the device enhanced the post-stall and deep stall lift coefficients. As the root of the LEAD was moved outboard from the wing root, the percent changes in lift coefficient with respect to the baseline increased. When the device was moved outboard of the location yielding the highest lift increase, the lift declined to its lowest value once the tip of the LEAD protruded outboard of the wingtip. Since each placement of the LEAD root affected the lift coefficient differently, the three-dimensional effects of the device are important under these flight conditions. In general, the LEAD root placement that yielded the best performance in this experiment was in the middle of the semi-span (50%), which was more outboard of the wing compared to the average alula location on type D avian wings. Since the test specimen was a uniform and rectangular wing, its airfoil distribution across the span

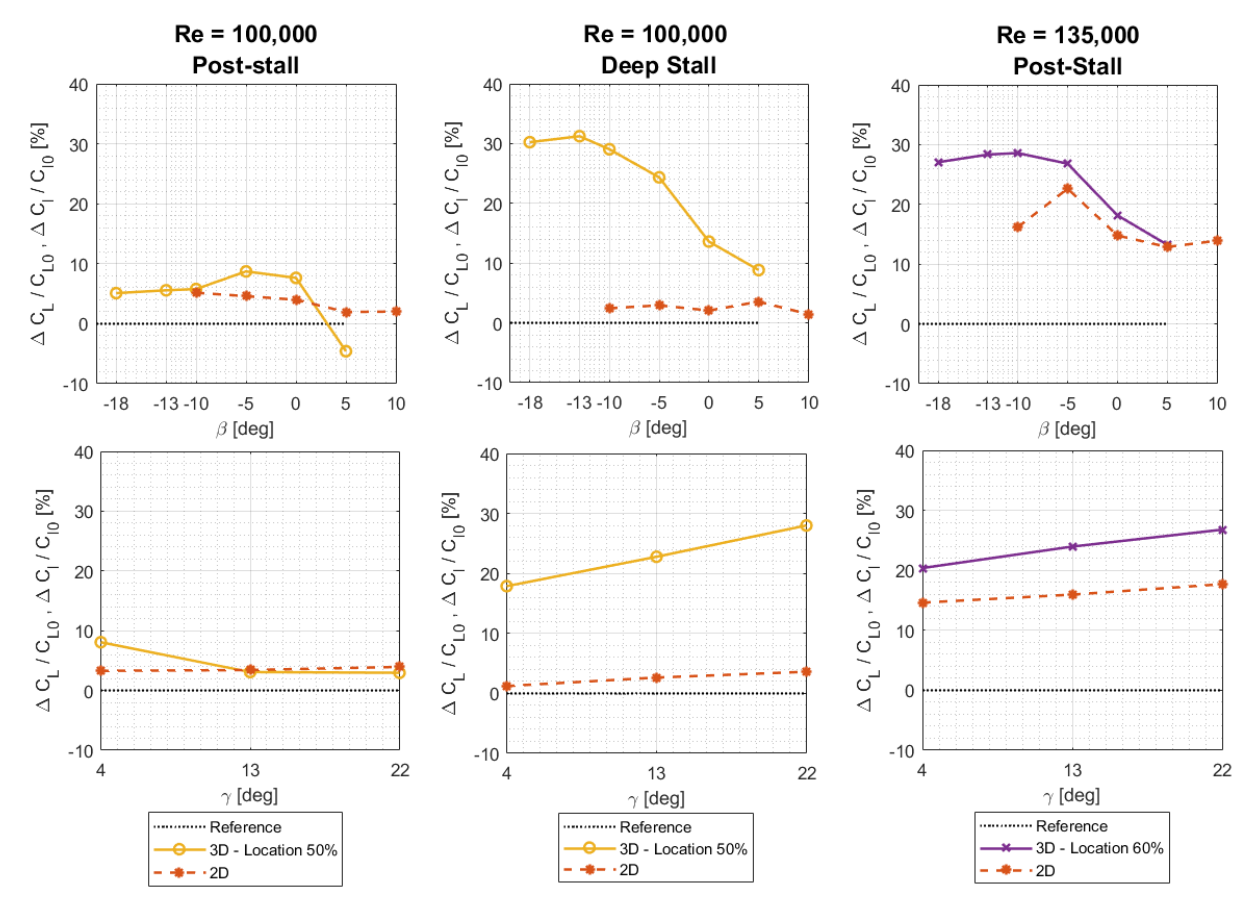


FIGURE 9. Comparison between lift percent differences generated by a LEAD on a wing (3D) and a LEAD on an airfoil (2D).

did not vary like bird wings (fig 1). In this experiment, the entire wing was more similar to the arm wing, which is the region with thicker airfoils; therefore, the LEAD achieved the highest lift enhancements at a location further outboard than the average alula location in avian wings. Lastly, based on the comparison between the three-dimensional and two-dimensional test results, the LEAD generated a higher lift increase on a finite wing than it did on an airfoil confirming that it is a three-dimensional device.

Based on the placement and deployment parameters that produced the highest lift enhancement, a small, flexible, and deployable LEAD structure can be developed. Since size and weight are great limitations on UAVs operating at low Reynolds numbers, a well-suited high lift device need to meet those criteria, as opposed to fixed, large, and heavier slats commonly seen on todays aircrafts. The development of a passively deployable structure calls for further understanding and modeling of low Reynolds number flow around a lifting surface.

6 CONCLUSION

This paper presented a Leading-Edge Alula-inspired Device (LEAD) lift-enhancement and stall-mitigation device for low to moderate aspect ratio (3D) wings at low Reynolds number. The aerodynamic effects of the device were evaluated through wind tunnel experiments on a high-lift cambered wing. Results show enhanced lift coefficients of up to 32% at post-stall and 37% at deep stall angles of attack. The percent change in lift generated by the rectangular 3D wing equipped with a LEAD, as compared to baseline, was sensitive to the spanwise placement of the device with respect to the wing root. The device also produced higher lift coefficients on a moderate aspect-ratio wing (3D) than it did on an airfoil (2D). These results prove that the LEAD is a threedimensional device and its spanwise placement is an important design parameter. The location resulting in the largest improvement was the middle of the semi-span. The correlations between aerodynamic performance, flow conditions, and best deployment parameters can be further developed and used to design an adaptive and deployable LEAD that can be implemented on a finite wing to increase mission-adaptability (i.e. expand the flight envelope).

ACKNOWLEDGMENT

The authors acknowledge support from the Mechanical Science and Engineering Department at the University of Illinois Urbana-Champaign.

REFERENCES

- [1] McCormick, B. W., 1994. Aerodynamics, Aeronautics, and Flight Mechanics, 2 edition ed. Wiley, New York, Sept.
- [2] Anderson, J. D. J., 2010. *Fundamentals of Aerodynamics*, 5 ed. McGraw-Hill Education, Feb.
- [3] Lissaman, P. B. S., 1983. "Low-Reynolds-Number Airfoils". Annual Review of Fluid Mechanics, 15(1), pp. 223–239.
- [4] Weyl, A. R., 1945. "HighLift Devices and Tailless Aeroplanes". *Aircraft Engineering and Aerospace Technology*, 17(10), Oct., pp. 292–297.
- [5] O. Smith, A. M., 1975. "High-Lift Aerodynamics". *Journal of Aircraft*, 12(6), June, pp. 501–530.
- [6] Abbott, I. H., and Doenhoff, A. E. V., 1959. *Theory of Wing Sections, Including a Summary of Airfoil Data*. Courier Corporation.
- [7] Rao, D., and Kariya, T., 1988. "Boundary-layer submerged vortex generators for separation control - An exploratory study". In *1st National Fluid Dynamics Conference*, Fluid Dynamics and Co-located Conferences. American Institute of Aeronautics and Astronautics, July.
- [8] Gen, M. S., Kaynak, ., and Lock, G. D., 2009. "Flow over an aerofoil without and with a leading-edge slat at a transitional Reynolds number". *Proceedings of the Institution of Mechanical Engineers, Part G: Journal of Aerospace Engineering*, 223(3), Mar., pp. 217–231.
- [9] Lee, S.-i., Kim, J., Park, H., Jaboski, P. G., and Choi, H., 2015. "The Function of the Alula in Avian Flight". *Scientific Reports*, 5, May.
- [10] Austin, B., and Anderson, A., 2007. "The Alula and Its Aerodynamic Effect on Avian Flight". In ASME 2007 International Mechanical Engineering Congress and Exposition, Vol. 7, ASME, pp. 797–806.
- [11] Meseguer, J., Franchini, S., Prez-Grande, I., and Sanz, J. L., 2005. "On the aerodynamics of leading-edge high-lift devices of avian wings". Proceedings of the Institution of Mechanical Engineers, Part G: Journal of Aerospace Engineering, 219(1), Jan., pp. 63–68.
- [12] Nachtigall, W., and Kempf, B., 1971. "Vergleichende Untersuchungen zur flugbiologischen Funktion des Daumenfittichs (Alula spuria) bei Vgeln". Zeitschrift fr vergleichende Physiologie, 71(3), Sept., pp. 326–341.
- [13] Savile, O. B. O. "Adaptive Evolution in the Avian Wing". *Evolution*, *11*(2), pp. 212–224.
- [14] Liu, T., Kuykendoll, K., Rhew, R., and Jones, S., 2006.

9

- "Avian Wing Geometry and Kinematics". *AIAA Journal*, 44(5), May, pp. 954–963.
- [15] Alvarez, J., Meseguer, J., Meseguer, E., and Perez, A., 2001. "On the role of the alula in the steady flight of birds". *Ardeola*, **48**(2), pp. 161–173.
- [16] Videlier, J. J., 2006. *Avian Flight*, 1 ed., Vol. 14 of *Oxford Ornithology Series*. Oxford University Press, Oct.
- [17] Mandadzhiev, B. A., Lynch, M. K., Chamorro, L. P., and Wissa, A. A., 2017. "An experimental study of an airfoil with a bio-inspired leading edge device at high angles of attack". *Smart Materials and Structures*, **26**(9), p. 094008.
- [18] Mandadzhiev, B. A., Lynch, M. K., Chamorro, L. P., and Wissa, A. A., 2016. "Alula-Inspired Leading Edge Device for Low Reynolds Number Flight". p. V002T06A016.
- [19] Carruthers, A. C., Walker, S. M., Thomas, A. L. R., and Taylor, G. K., 2010. "Aerodynamics of aerofoil sections measured on a free-flying bird". *Proceedings of the Institution of Mechanical Engineers, Part G: Journal of Aerospace Engineering*, 224(8), Aug., pp. 855–864.
- [20] Selig, M., Guglielmo, J., Broeren, A., and Giguere, P., 1995. *Summary of Low-Speed Airfoil Data*, Vol. 1. SoarTech.